UCRL--101516

DE90 007250

Direct Implicit Simulation of Collisionless Magnetic Reconnection

Gregory E. Francis, Dennis W. Hewett, and Claire E. Max

Institute of Geophysics and Planetary Physics
Lawrence Livermore National Laboratory
University of California

Abstract

Collisionless reconnection of magnetic field lines depends upon electron inertia effects and details of the electron and ion distribution functions, thus requiring a kinetic description of both. Though traditional explicit PIC techniques provide this description in principle, they are severly limited in parameters by time step constraints. This parameter regime has been expanded in this work by using the recently constructed 2.5 D electromagnetic code AVANTI. The code runs stably with arbitrarily large Δt and is quite robust with respect to large fluctuations occurring due to small numbers of particles per cell. We find excellent agreement with linear electron tearing theory for early simulation times, provided electrostatic effects are included in the theory. In the non-linear regime following tearing, we observe electrostatic ringing of electrons and trapped flux into the magnetic island, superposed on linear growth determined by the ion sound velocity. It is found that the inclusion of a guide magnetic field (magnetic shear) severely slows the initial stages of reconnection and damps out the electrostatic ringing if local values of the guide field are above a threshold determined by questions of electron mobility.

---

1. Introduction

We report here continued research [*Hewett et al., 1988*] on the evolution of magnetic field reconnection in a collisionless plasma neutral sheet, using implicit particle-in-cell computer simulations. The general two-dimensional collisionless neutral sheet configuration is thought to be of relevance to the magnetotails of the earth and other magnetized planets, where reconnection is associated with magnetic sub-storms [*Coroniti and Kennel, 1972; Russell and McPherron, 1973; Schindler, 1980*]; and to the eventual fate of tangled magnetic field lines in collisionless astrophysical plasmas, in which estimates of the thermal conductivity depend sensitively on the largely unknown rate of field-line reconnection [*Cowie and McKee, 1977*]. The specific parameters of our simulation are quite close to plasma conditions in the laboratory reconnection experiments of Stenzel and Gekelman [*Stenzel and Gekelman, 1981; Gekelman and Stenzel, 1981*].

In simplest form reconnection in a *collisional* plasma can be modeled using the MHD equations with a fixed value for the plasma resistivity. This yields a reduced, one-fluid description in which the large-scale topology and dynamics of reconnecting regions can be studied. By contrast, *collisionless* reconnection of magnetic field lines depends on electron inertia effects and the detailed behavior of the electron distribution function to provide the necessary freedom for magnetic topology changes. The formation of a non-Maxwellian tail on the ion distribution can be an important observed consequence of collisionless reconnection. Hence a faithful computational model must include a kinetic description of both electrons and ions.

Although traditional explicit particle-in-cell (PIC) techniques provide this description, stability requirements restrict the time step to such small values that computer constraints limit the simulation either to short temporal periods (e.g. 100 plasma periods ω_{pe}^{-1} or less), or to artificially small ion-to-electron mass ratios (e.g. $M_i/m_e \approx 10$ to 25) [*Leboeuf et al., 1982; Leboeuf et al., 1984; Hoshino, 1987*]. In the present paper a new 2.5D fully electromagnetic Direct Implicit PIC plasma simulation code AVANTI [*Hewett and Langdon, 1987*] allows us to follow the dynamics of collisionless reconnection for all relevant M_i/m_e, and for a factor of 2 to 3 longer timescales. The code runs stably with arbitrarily large Δt and is quite robust with respect to large fluctuations occurring due to small numbers of particles per cell.

This code is ideally suited for studies of magnetic reconnection because of the increased flexibility in time step selection. High frequency plasma behavior that proves immaterial to magnetic reconnection need not be resolved numerically. For example, neither purely electromagnetic modes or electron plasma oscillations are important in this process and are not resolved. We select the appropriate time step, typically $\omega_{pe}\Delta t \approx$ 1-2, needed to give detailed resolution of electron gyro-motion and other particle-field interactions that are important to collisionless reconnection. Further details of this method can be found in *Hewett and Langdon* [*1987*] and references therein. Overall, we estimate that this implicit technique has expanded the parameter regime that can be studied by at least an order of magnitude.

The simulation region consists of a 40x96 x-y mesh, with all quantities initially uniform in y. Starting with a constant ion temperature and a Gaussian ion density profile we derive the initial equilibrium fields shown in Figure 1(a). The initial neutral sheet width δ is $2c/\omega_{pe}$. Larmor radii for electrons and ions outside of the neutral sheet are $\rho_e = 0.4c/\omega_{pe}$ and $\rho_i = 20c/\omega_{pe}$, respectively. By way of comparison, the laboratory reconnection experiments of *Stenzel and Gekelman* [*1979*] typically use $\delta = 3c/\omega_{pe}$, $\rho_e = 0.4c/\omega_{pe}$ and $\rho_i = 2c/\omega_{pe}$. The x-gradient in magnetic pressure near the neutral sheet is balanced by gradients in electron and ion particle density. Periodic boundary conditions are imposed at the top and bottom of the box. At the sides of the box, fields and particle densities approach values that are constant with x. Boundary conditions at the sides are perfect reflection for particles, Dirichlet conditions for **E**, and Neumann conditions for **B**.

This equilibrium resembles the Harris equilibrium, [*Harris, 1962*] but the ions carry no current, and are electrostatically confined. We also allow for anisotropy in electron temperatures parallel ($T_{e\|}$) and perpendicular ($T_{e\perp}$) to the initial magnetic field. Following the work of *Chen and Palmadesso* [*1984*], we allow a cooler $T_{e\|}$ to trigger the initial stages of reconnection.

2. Simulation Results

Figure 1(b-d) shows the time evolution of the magnetic field topology for a typical simulation. Contours of magnetic flux are shown as solid lines; the

dotted contour is the "separatrix", inside of which lies magnetic flux that has become trapped due to reconnection. Frame 1(b) shows the magnetic configuration characteristic of the early stages of reconnection, before the ions have had time to move. The electron current at the neutral sheet has already formed small-scale filaments, resulting in several magnetic X-points within the simulation volume. Later, Figure 1(c) shows that some of these small-scale filaments have coalesced. Still later, when enough time has passed for ion dynamics to become important, we see one remaining magnetic island, as in Figure 1(d). This stage of the process is typically reached in approximately 1-3 Alfvén transit times. The remaining O-point continues to grow in amplitude, for our parameters, until the separatrix approaches the boundaries of the simulation box. The simulation is then terminated; further results would be artifacts of the boundary conditions.

A current-aligned component of the electric field (E_z) develops as the small-scale current filaments coalesce; this field is consistent with the $\mathbf{E} \times \mathbf{B}$ drift of the electrons (but not the unmagnetized ions) into the final O-point through the X-point. The resulting electron current in the x-y simulation plane generates a current-aligned component of the magnetic field (B_z) with quadrupole structure. Shown in Fig. 2 are the a) contours of E_z and b) B_z at the same time as Fig. 1d contours. It has been shown [*Hoshino, 1987*] that the suppression of this quadrupole field does not affect the rate of magnetic reconnection, suggesting that B_z is not a cause, but an effect, of the reconnection process.

Simulations with large ion-electron mass ratio ($M_i/m_e \geq 200$) reveal an oscillation in the sign of the current-aligned B_z quadrupole. The cause is an oscillation in the electron flow through the X-point. Since the magnetic field is "frozen" into the electron component, the magnitude of trapped magnetic flux will also oscillate as the electrons flow into and out of the O-point. Observation of trapped flux as a function of time for various M_i/m_e provides information about the moderating influence of the ions on the electron oscillation. This temporal behavior is consistent with the ions attempting to follow the electrons into the O-point, pulled by an ambipolar electric field. For large ion-to-electron mass ratios (> 200), the electron flow reverses before the ions can neutralize the excess electronic charge. These curves are shown in Figure 3 for six different values of M_i/m_e.

Late in time after the oscillations damp out, the trapped flux grows

approximately linearly in time, at a rate proportional to the ion-acoustic speed, $v_s = (kT_e/M_i)^{1/2}$. (Consistent with this scaling, in the limit $M_i/m_e \rightarrow \infty$ the trapped flux experiences simple oscillation with no secular growth.) This late-time oscillation and secular growth of trapped flux is a qualitatively different phenomenon than has been reported in previous studies [*Leboeuf et al., 1982; Hoshino, 1987*]. Previous investigators, using M_i/m_e=10–25, saw the coalescence of small-scale magnetic islands and sometimes saw oscillatory behavior, but after the island began to interact with the outer wall. Inadequate separation between the ion and electron timescales would obscure the late time oscillations that we see resulting from charge separation electric fields and from $\mathbf{E} \times \mathbf{B}$ forces, superposed on continued secular growth of trapped flux (Fig. 3).

The nature of the three temporal regions described above for $M_i/m_e > 200$ can be clarified by an idealized simulation having $T_{e\|}/T_{e\perp} = 0$, and $M_i/m_e = 2000$. Figure 4 shows the time evolution of a) trapped magnetic flux, b) quadrupole z component of magnetic field, c) electron flow energy in the y- and z-directions, and d) z components of electric field and current. Region I, in which the trapped flux grows linearly with time, corresponds to the early electron-driven formation of small-scale current filaments as evidenced in Figure 1(b). Region II corresponds to the coalescence of the small-scale multiple X-points, and shows exponential growth of trapped flux. The end of region II is signaled by a peak in y-directed electron energy (Fig. 4c)consistent with jetting, and a corresponding reduction of the z-directed energy caused by the E_z required for the jetting. In Region III, ions play the decisive role: an ambipolar electric field between the electrons and much-more-massive ions reverses the electron flow, causing oscillations back and forth from the external region through the X-point to the O-point. These oscillations are seen most clearly in Figure 4(b).

The oscillations that are evident in the z component of the electric field, Figure 4(d), are not found in the z component of the current. In fact there is no proportionality at all between the time behaviors of E_z and J_z. The z components of the current and electric field do not even occupy the same volume in our simulations. Early in the reconnection process the electrons that carry J_z move away from the X-points, and subsequent currents flow in the vicinity of the O-points. This behavior is seen in laboratory reconnection experiments as well [*Gekelman and Pfister, 1987*].

Even if there were an "anomalous resistivity" η, the rate of dissipation ηJ^2 would be quite small at the X-point, since J_z is small there. Thus the MHD picture with an "anomalous resistivity" η acting on the z-component of current at the X-point seems to be qualitatively incorrect for the cases we have examined here.

The distinction between regions I and II in Figure 4 is the linear, rather than exponential, growth of trapped flux at early time. Previous speculation [*Hewett et al., 1988*] that the distinction is *not* due to the extreme initial anisotropy ($T_{e\|}/T_{e\perp} = 0$) has been proven. Shown in Figure 5(a) are plots of trapped flux for two runs starting with anisotropies having the extreme value of 0 and our canonical value of 4/9. The qualitative similarity of the two simulations throughout the run and especially in the early time surrounding regions I and II affirm our early speculation.

The second more likely possibility for the distinction between regions I and II is that the large fluctuation noise is associated with the limited number of simulation particles ($N_e = N_i = 27{,}000$). This noise provides very early "reconnection" with sufficient amplitude to obscure the early exponential growth. Simulation of this problem with ($T_{e\|}/T_{e\perp} = 4/9$) and an order of magnitude more particles ($N_e = N_i = 216{,}000$) does indeed show exponential growth (Fig. 5b) and the absence of the linear growth of region I. Further, we find the exponential growth to be consistent with the linear collisionless electron-driven tearing mode instability [*Coppi et al., 1966;Laval et al., 1966*], providing consideration is made in the theory for the inclusion of the electrostatic effects [*Katanuma and Kamimura, 1980; Hoshino, 1987*].

The evidence is that simple fluctuations near the field null cause small scale islands to form with amplitudes proportional to the initial particle noise level. These early islands, through not the most unstable length in y, dominate the simulation until the exponential growth of the most unstable island length overtakes the growth of the early perturbations. Large numbers of simulation particles suppress the initial noise-related perturbations and exhibit only exponential growth of the most unstable mode. This result is further supported by examining the Fourier spectrum in y of B_z in Fig. 6 that shows the linearly-predicted most unstable mode dominating the mode with one-half the wavelength.

We note that the simulation with fewer particles displays excellent qual-

itative agreement (see Fig. 5b) for those phenomena occurring in the non-linear regime–providing confidence for further study with relatively inexpensive simulations using fewer simulation particles.

3. Magnetic Shear

The addition of a zeroth-order magnetic field aligned with the sheet current retains most of the features of the simulations just described. We report here the findings of an on-going parametric study of the effects of magnetic shear on the reconnection process. The magnetic shear is introduced through the inclusion of a zero order dc magnetic field in the z-direction which is initially taken to be uniform across the simulation plane. We began this study in an attempt to connect our previous findings without shear to problems in laboratory plasmas, such as tokamaks, compact toroids, reversed-field pinches, and the reconnection experiments of *Stenzel and Gekelman* [*1979*]. In these systems magnetic reconnection takes place in the presence of magnetic shear.

In Figure 7 we plot the time histories of trapped flux for four different values of the initial guide magnetic field B_{z0}. The first thing to be noted from Figure 7 is that much of the basic physics involved in collisionless magnetic reconnection appears to be unaffected by the inclusion of a guide magnetic field. Of note are two exceptions to this observation. First, there appears to be a discontinuous, or at least non-linear, decrease in the initial growth rate between the simulation runs having $B_{z0} = B_0 \equiv 0.12$ and $B_{z0} = 2B_0$. This can be understood by looking at the threshold for B_{z0}, above which the electrons in the neutral sheet are no longer un-magnetized. We define this threshold B_{zc} such that the electron Larmor radius in the neutral sheet $\rho_e(x = 0)$ is equal to the geometric mean of the neutral sheet width δ and the electron Larmor radius outside of the neutral sheet $\rho_e(x >> \delta)$:

$$\rho_e(x = 0) = \sqrt{\delta \rho_e(x >> \delta)}, \quad \text{for } B_{z0} = B_{zc}. \tag{1}$$

This calculation yields a critical guide field of $B_{zc} = 0.18$, above which the neutral sheet electrons are magnetized and no longer free to stream. Note

that this critical value of B_{z0} lies halfway between that of the two runs in question.

The second point to make from Figure 7 is that the electrostatic ringing is apparently unaffected by the transition above B_{zc}: the amplitude of the oscillation of electrons and magnetic flux into and out of the magnetic island is just as large for the case $B_{z0} = 2B_0 > B_{zc}$ as it is for $B_{z0} = B_0 < B_{zc}$. It is not until B_{z0} is raised to $4B_0$ ($>> B_{zc}$) that the electrostatic ringing is damped away by the increased viscosity in the system. Since the ringing is a manifestation of electron jetting (free streaming into the O-point), we would not expect to see the ringing above B_{zc}. To explain this apparent discrepancy, we look at a contour map of guide magnetic field for the case $B_{z0} = 2B_0$ (see Fig. 8a). We find that as electrons are gathered and heated inside of a magnetic island, the B_z in the island is reduced from its initial uniform value B_{z0}. This "hollowing out" of the guide magnetic field at an island is due to a Kelvin-Helmholz instability that drives electron current around the perimeter of the magnetic island. Figure 8(a) shows that at the time $t = 410\omega_{pe}^{-1}$, when the $B_{z0} = 2B_0$ case is making the transition between the exponential growth of the electron tearing mode and the linear growth of the ion-mediated reconnection, the guide field in the magnetic island has been reduced through this hollowing-out process to values below the threshold B_{zc}, thus allowing the neutral sheet electrons to jet. A similar map for the case $B_{z0} = 4B_0$ shows that the guide field is not reduced below the threshold at the time of transition, hence the electrostatic ringing is damped.

4. Discussion

The results of the present work agree qualitatively with behavior seen in previous computer simulations at early and intermediate times : 1) initial formation of small-scale magnetic islands, and 2) rapid coalescence of these into larger structures, with concomitant development of a driving E_z. We observe a new type of behavior at later times, for ion-to-electron mass ratios above 200: oscillatory electron currents through the X-point in the x-y plane, superimposed on linear (not exponential) growth of trapped flux at a rate proportional to $(T_e/M_i)^{1/2}$.

Our simulations indicate that the region showing oscillatory behavior (Region III of Fig. 4a) is one in which an electron current flows into and out of the O-points through the X-points. The ions attempt to follow the electron current, pulled by an ambipolar electric field. But only for small ion-to-electron mass ratios (< 200) can they succeed in doing so before the electron flow reverses. Such behavior emphasizes that in our simulations the magnetic flux is frozen into the *electron* component rather than the plasma as in the usual MHD formulation.

Near the end of our simulation the growth of trapped flux occurs with one dominant mode in B_x, because shorter wavelength modes have already undergone coalescence. Thus theories of nonlinear saturation which rely on the presence of many modes in k-space [*Coroniti, 1977; Biskamp et al., 1970*] are not applicable here. The late-time amplitudes are large in our simulations: $\langle B_x \rangle / B_0 \sim (\sqrt{2}\rho_e/\delta)^1 \sim 0.3$ at time $600\omega_{pe}^{-1}$. In addition, $\langle B_x \rangle$ continues to increase at late times in the simulation, with trapped flux growing linearly with time. This late-time continued growth, which has not been reported in previous particle-in-cell computer simulations, qualitatively resembles the Sweet-Parker phase predicted for MHD reconnection [*Parker, 1979*], and would be a particularly interesting case for further analysis.

Generally, the sheared magnetic field configuration displays much of the behavior observed in the nonsheared studies. In particular, spontaneous reconnection can occur in both cases; it can be characterized as having three regimes; and with small enough B_{z0}, can exhibit the late time oscillation of the trapped flux mediated by the ion mass. In some cases, however, the plasma is unable to mimic zero-shear behavior until it has expelled enough B_z so that local values are below thresholds determined by questions of electron mobility. We find, in particular, that the rapid coalescence of small filaments into large current channels at the O-points are inhibited until the B_z field along the original B_y field null is suitably reduced. Similarly, the zero-shear simulations exhibited flux oscillations as the un-magnetized electrons respond to $\mathbf{E} \times \mathbf{B}$ and ambipolar forces. We find that with strong shear this oscillation is inhibited unless the local field is below a threshold B_{zc}.

This research was performed under the auspices of the U.S. Department of Energy by the Lawrence Livermore National Laboratory under contract no. W-7405-ENG-48.

References

Biskamp, D., R.Z. Sagdeev, and K. Schindler, Nonlinear evolution of the tearing instability in the geomagnetic tail, Cosmic Electrodynamics **1**, 297 (1970).

Chen, J., and P. Palmadesso, Tearing instability in an anisotropic neutral sheet, Phys. Fluids **27**, 1198 (1984).

Coppi, B., G. Laval, and R. Pellat, Dynamics of the geomagnetic tail, Phys. Rev. Lett., **16**, 1207 (1966).

Coroniti, F.V., and C.F. Kennel, Polarization of the auroral electrojet, J. Geophys. Res. **77**, 3361 (1972).

Coroniti, F.V., Nonlinear evolution of the collisionless tearing mode, Phys. Rev. Lett. **38**, 1355 (1977).

Cowie, L.L., and C.F. McKee, The evaporation of spherical clouds in a hot gas, 1. Classical and saturated mass loss rates, Astrophys. J. **211**, 135 (1977).

Gekelman, W., and H. Pfister, Experimental observation and theoretical analysis of the tearing mode in an electron current sheet, Bull. Am. Phys. Soc. **32**, 1753 (1987).

Gekelman, W., and R.L. Stenzel, Magnetic field line reconnection experiments 2. Plasma parameters, J. Geophys. Res. **86**, 659 (1981).

Harris, E.G., On a plasma sheath separating regions of oppositely directed magnetic field, Nuovo Cimento **23**, 115 (1962).

Hewett, D.W., G.E. Francis, and C.E. Max, New regimes of magnetic reconnection in collisionless plasmas, Phys. Rev. Lett. **61**, 893, August 15, (1988).

Hewett, D.W., and A.B. Langdon, Electromagnetic direct implicit plasma simulation, J. Comp. Phys. **72**, 121 (1987).

Hoshino, M., The electrostatic effect for the collisionless tearing mode, J. Geophys. Res. **92**, 7368 (1987).

Katanuma, I., and T. Kamimura, Simulation studies of the collisionless tearing instabilities, Phys. Fluids **23**, 2500 (1980).

Laval, G., R. Pellat, and M. Vuillemin, Instabilités electromagnétiques des plasmas sans collisions, in *Plasma Physics and Controlled Nuclear Fusion Research*, Vol. 2, p.259, (I.A.E.A., Vienna, 1966).

Leboeuf, J.N., T. Tajima, and J.M. Dawson, Dynamic magnetic X points, Phys. Fluids **25**, 784 (1982).

Leboeuf, J.N., F. Brunel, T. Tajima, J. Sakai, C.C. Wu, and J.M. Dawson, Computer modeling of fast collisionless reconnection, in *Magnetic Reconnection in Space and Laboratory Plasmas*, edited by E.W. Hones (Am. Geophys. Union, Washington DC, 1984), pg. 282.

Parker, E.N., *Cosmical Magnetic Fields*, (Clarendon Press, Oxford, 1979), chapter 15.

Russell, C.T., and R.L. McPherron, The magnetotail and substorms, Space Sci. Rev. **15**, 205 (1973).

Schindler, K., in *Dynamics of the Magnetosphere*, edited by S.-I. Akasofu (Reidel, Hingham, Mass., 1980), page 311.

Stenzel, R.L., and W. Gekelman, Experiments on magnetic field-line reconnection, Phys. Rev. Lett. **42**, 1055 (1979).

Stenzel, R.L., and W. Gekelman, Magnetic field line reconnection experiments 1. Field topologies, J. Geophys. Res. **86**, 649 (1981).

Figure Captions

Figure 1. a) Profiles of initial electrostatic field E_x (dashed) and magnetic field B_y (solid) across the neutral sheet. Both fields have units of $m_e c\omega_{pe0}/e$. The sheet current in the z direction is carried by electrons. Ions are contained by the electrostatic field. The initially uniform electron and ion temperatures are $T_{e\perp}/m_e c^2 = 2.8 \times 10^{-2}$, $T_{e\parallel} = (4/9)T_{e\perp}$, $T_i/m_e c^2 = 8.0 \times 10^{-2}$. (b-d): Magnetic flux contours (solid) and separatrix (dotted) in x-y plane: (b) At $t = 30\omega_{pe}^{-1}$, showing small-scale electron-driven filaments; (c) At $t = 160\omega_{pe}^{-1}$, as coalescence begins; (d) At $t = 410\omega_{pe}^{-1}$, with only one X-point remaining.

Figure 2. The current-aligned component of the (a) electric field at time $t = 240\omega_{pe}^{-1}$, consistent with the magnetic flux configuration of Fig. 1d and (b) the magnetic quadrupole structure of the current-aligned component of the magnetic field for the same time.

Figure 3. Trapped magnetic flux vs time, for six different M_i/m_e. In all cases, $T_{e\parallel}/T_{e\perp} = 4/9$ initially. The long-time linear growth is proportional to $M_i^{-1/2}$.

Figure 4. Time evolution of an idealized simulation with initial $T_{e\parallel}/T_{e\perp} = 0$ and $M_i/m_e = 2000$: (a) trapped magnetic flux; (b) peak-to-peak amplitude of quadrupole magnetic field B_z; (c) electron flow energy in the y- and z-directions versus time; and (d) E_z (dots) and J_z (triangles) at the y-position of the X-point, averaged over x.

Figure 5. Trapped magnetic flux vs time with (a) all parameters equal except for different $T_{e\parallel}/T_{e\perp}$. Shown in (b) is a comparison with $T_{e\parallel}/T_{e\perp} = 4/9$ but with one run having an order of magnitude more particles.

Figure 6. Time histories of the Fourier amplitudes for the many particle run shown in Fig. 5b. The most unstable mode $k_y = 0.2\omega_{pe}/c$ clearly dominates the mode with half the wavelength $k_y = 0.4\omega_{pe}/c$ that appears to be the most unstable early in the high noise runs (as in Fig. 1b).

Figure 7. Trapped magnetic flux vs time for four different values of the initial guide magnetic field B_{z0}. Electrons in the neutral sheet are strongly magnetized for $B_{z0} \geq 0.18$.

Figure 8. a) Contour map of the guide magnetic field at time $t = 410\omega_{pe}^{-1}$ for the case $B_{z0} = 2B_0 = 0.24$ of Fig. 4. The field inside of the island is below the threshold B_{zc}. b) Magnetic flux contours at the same time indicating the position of the magnetic island.

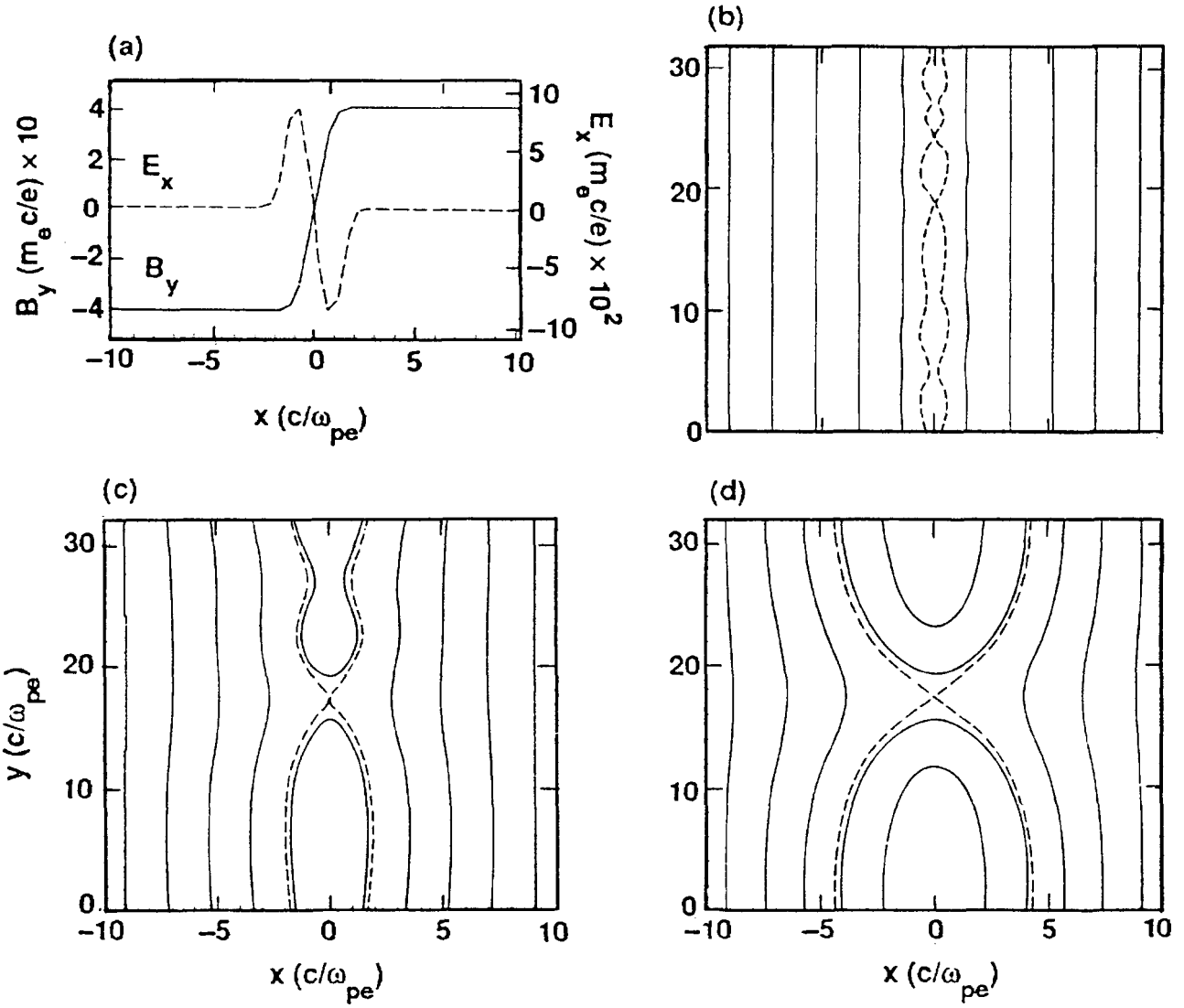
(a)
B_y ($m_e c/e$) × 10
E_x ($m_e c/e$) × 10^2
E_x
B_y
x (c/ω_{pe})
(b)
(c)
y (c/ω_{pe})
x (c/ω_{pe})
(d)
x (c/ω_{pe})

Figure 1

a)

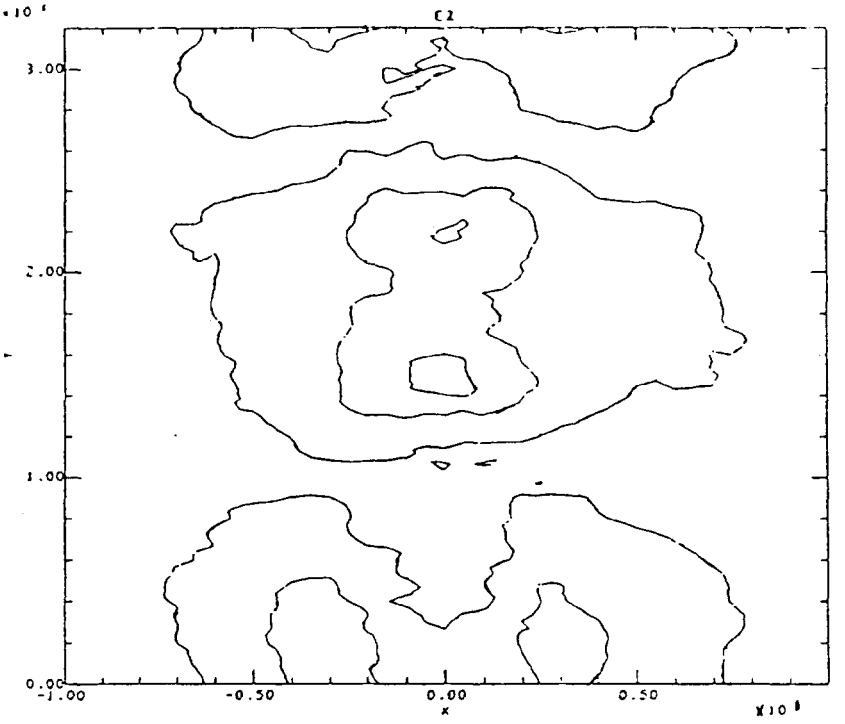
E2
3.00
2.00
1.00
0.00
-1.00
-0.50
0.00
0.50

b)

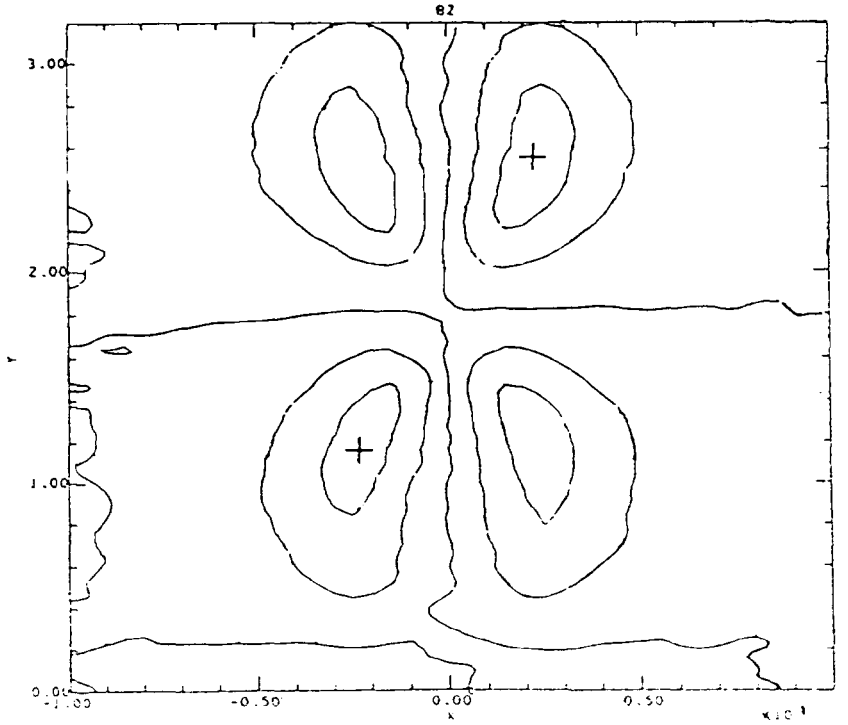
B2
3.00
2.00
1.00
0.00
-1.00
-0.50
0.00
0.50

Fig 2

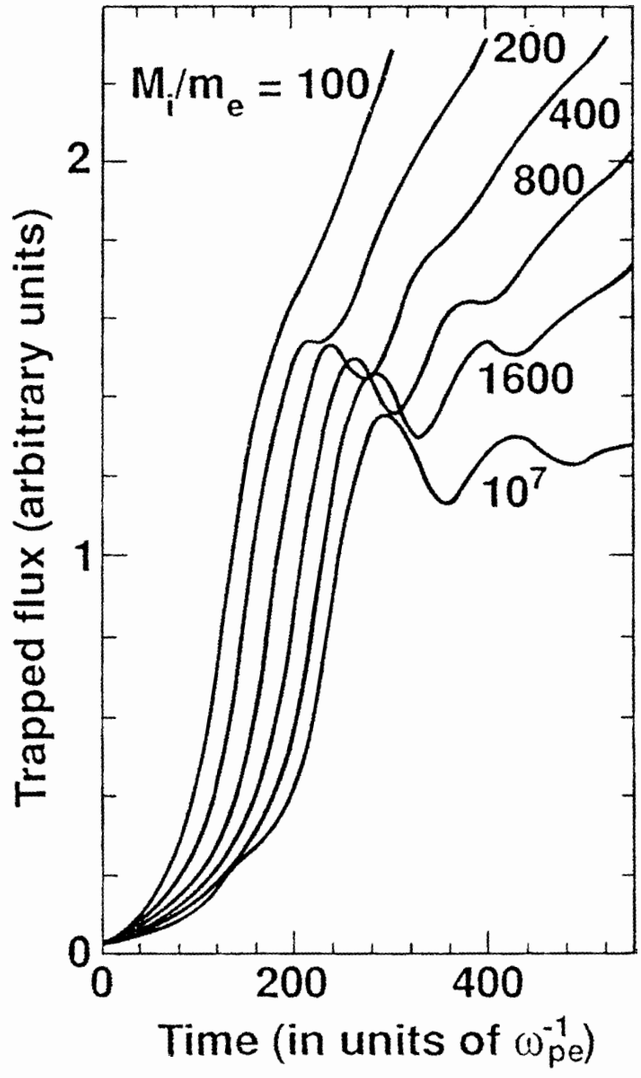
M_i/m_e = 100
200
400
800
1600
10^7
Trapped flux (arbitrary units)
0
1
2
0
200
400
Time (in units of ω_{pe}^{-1})

Figure 3

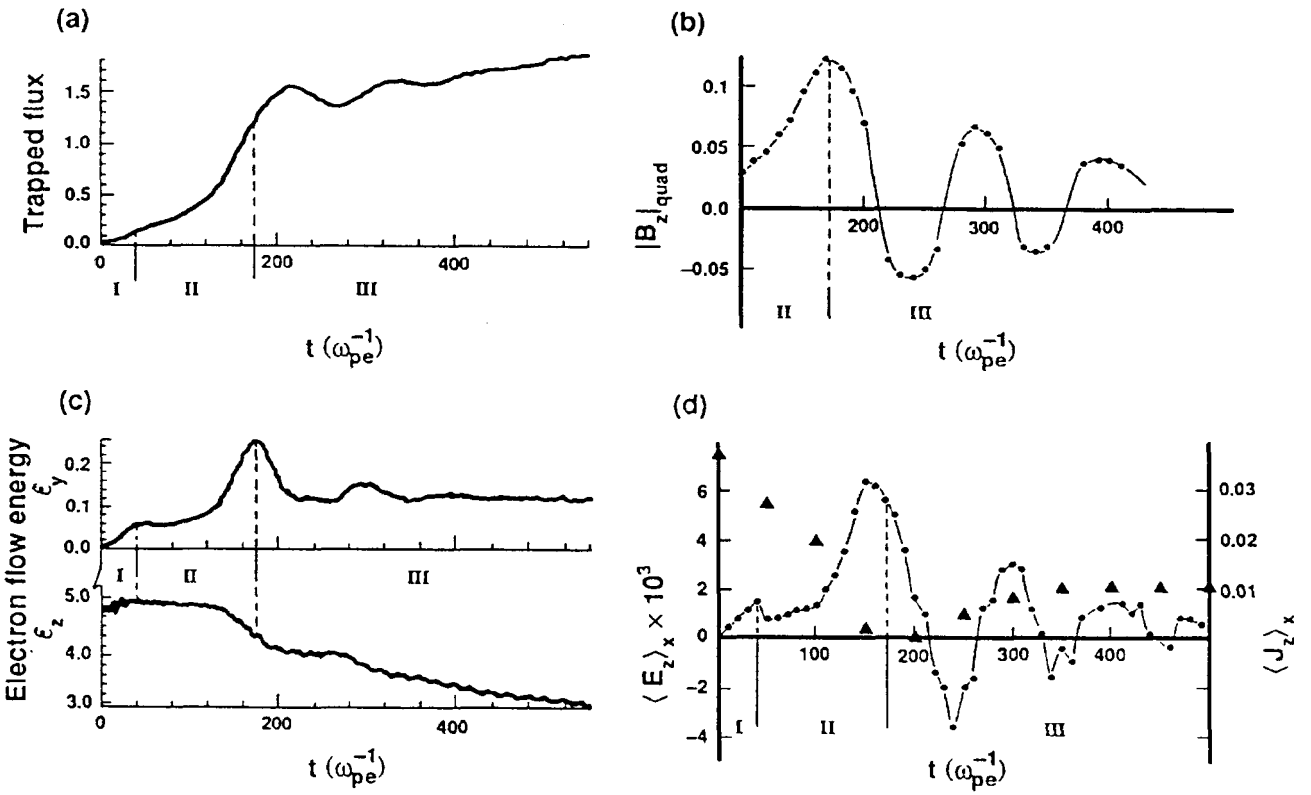
(a)
Trapped flux
1.5
1.0
0.5
0.0
0
200
400
I
II
III
t (ω_{pe}^{-1})
(b)
$|B_z|_{quad}$
0.1
0.05
0.0
−0.05
200
300
400
II
III
t (ω_{pe}^{-1})
(c)
Electron flow energy
ϵ_y
0.2
0.1
0.0
I
II
III
ϵ_z
5.0
4.0
3.0
0
200
400
t (ω_{pe}^{-1})
(d)
$\langle E_z \rangle_x \times 10^3$
6
4
2
0
−2
−4
100
200
300
400
I
II
III
0.03
0.02
0.01
$\langle J_z \rangle_x$
t (ω_{pe}^{-1})

Fig 4

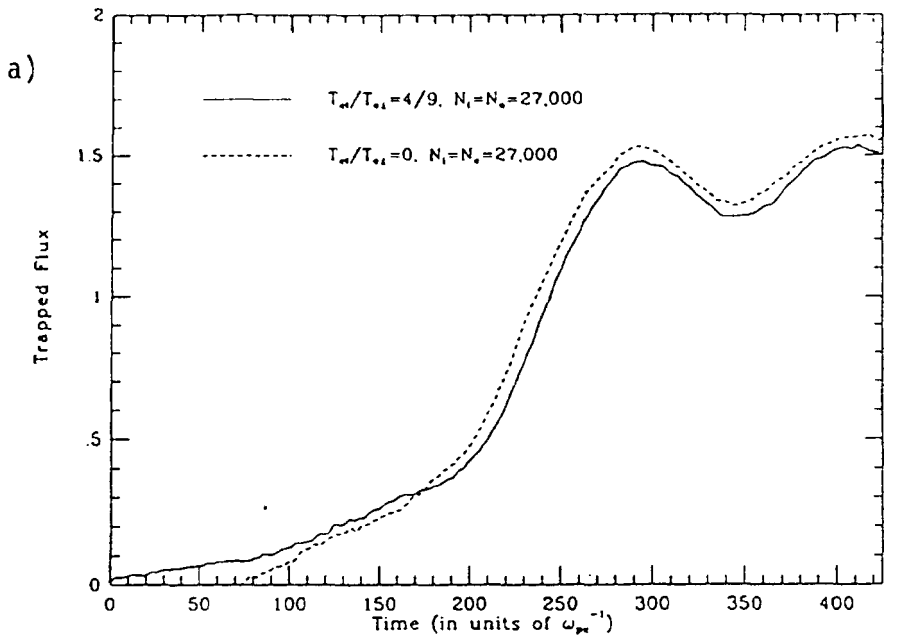
a)
T_{el}/T_{el}=4/9, $N_i=N_e$=27,000
T_{el}/T_{el}=0, $N_i=N_e$=27,000
Trapped Flux
Time (in units of ω_{pe}^{-1})

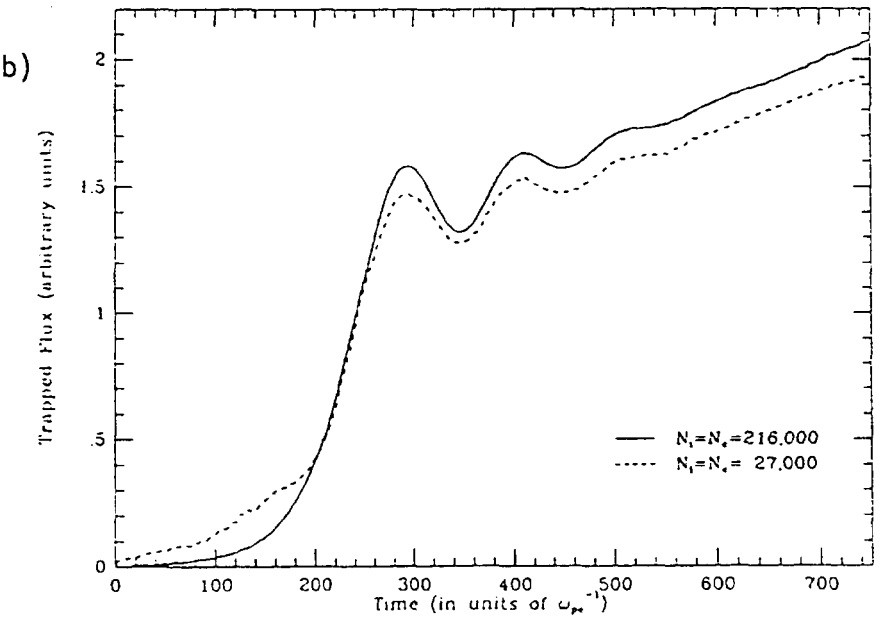
b)
Trapped Flux (arbitrary units)
$N_i=N_e$=216,000
$N_i=N_e$= 27,000
Time (in units of ω_{pe}^{-1})

Fig. 5

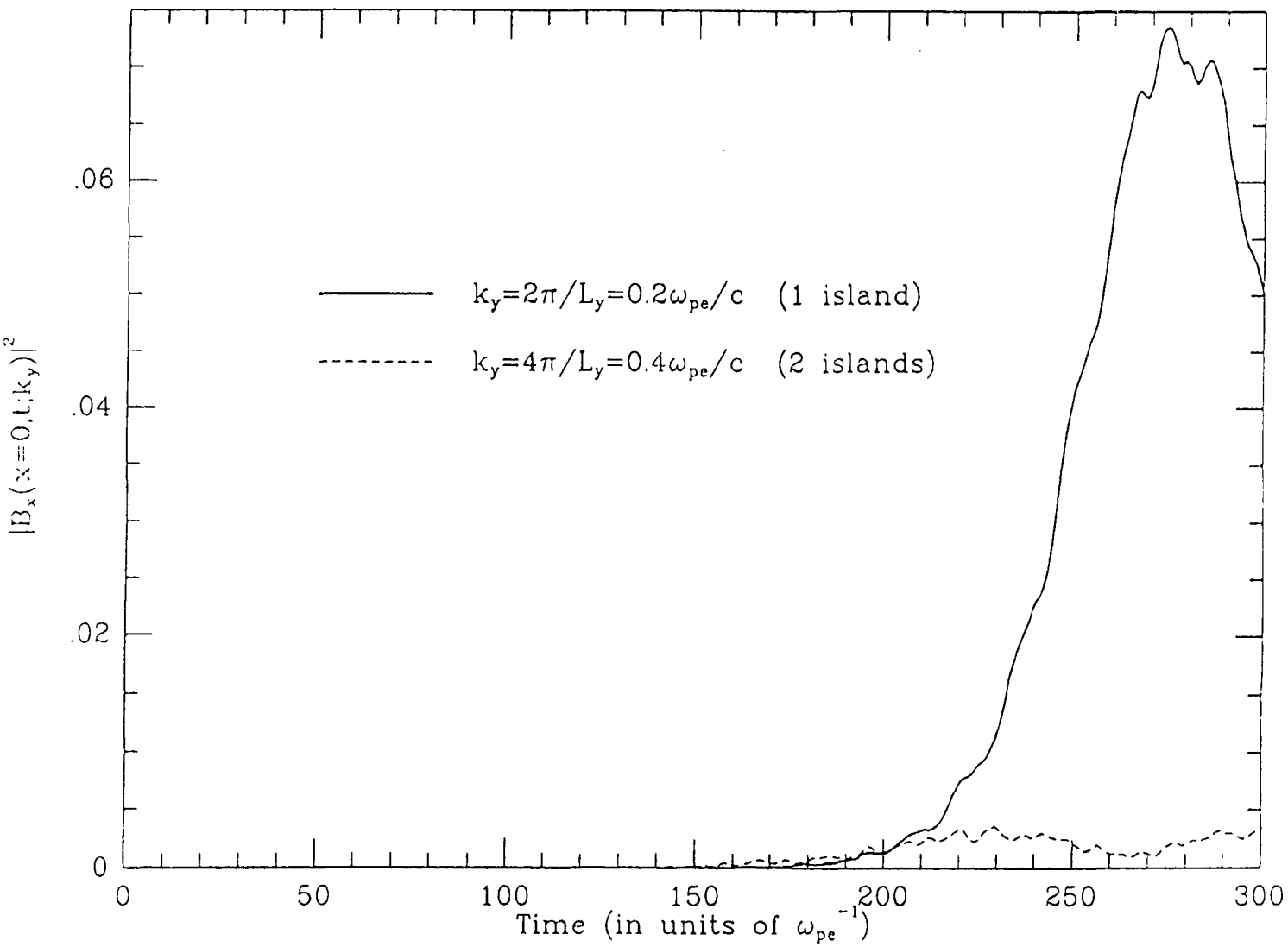
.06
.04
.02
0
0
50
100
150
200
250
300
Time (in units of ω_{pe}^{-1})
$|B_x(x=0,t;k_y)|^2$
$k_y=2\pi/L_y=0.2\omega_{pe}/c$ (1 island)
$k_y=4\pi/L_y=0.4\omega_{pe}/c$ (2 islands)

Fig. 9

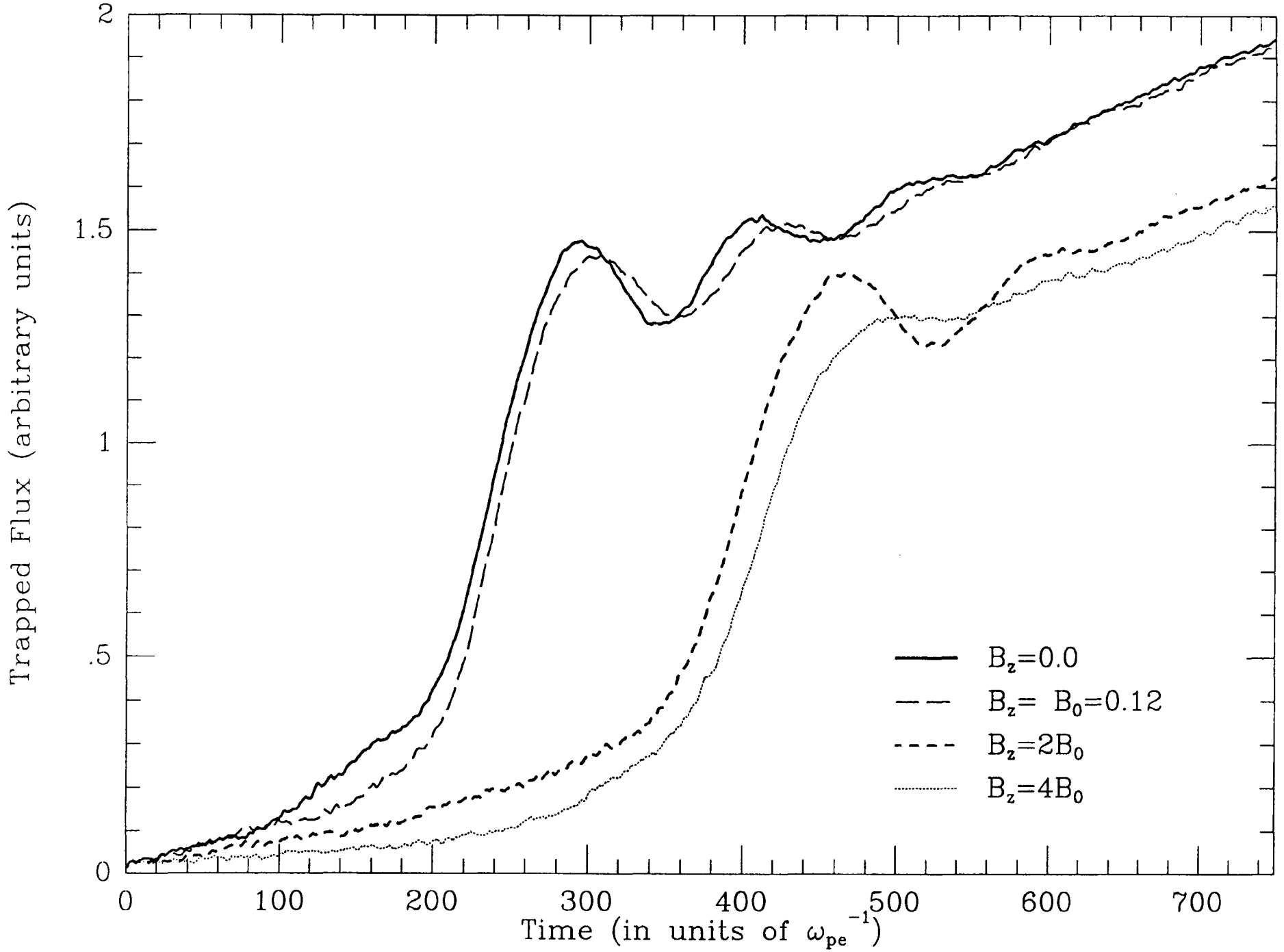
Trapped Flux (arbitrary units)
Time (in units of ω_{pe}^{-1})
0
.5
1
1.5
2
0
100
200
300
400
500
600
700
B_z=0.0
B_z= B_0=0.12
B_z=2B_0
B_z=4B_0

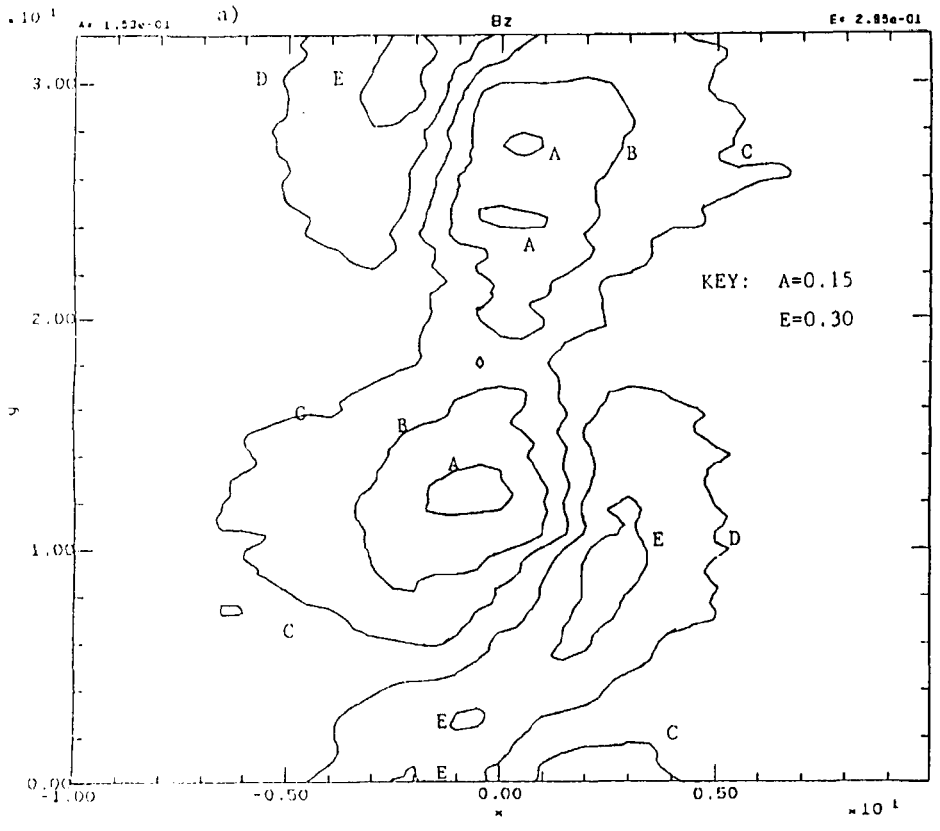
a)
Bz
KEY: A=0.15
E=0.30
x
y

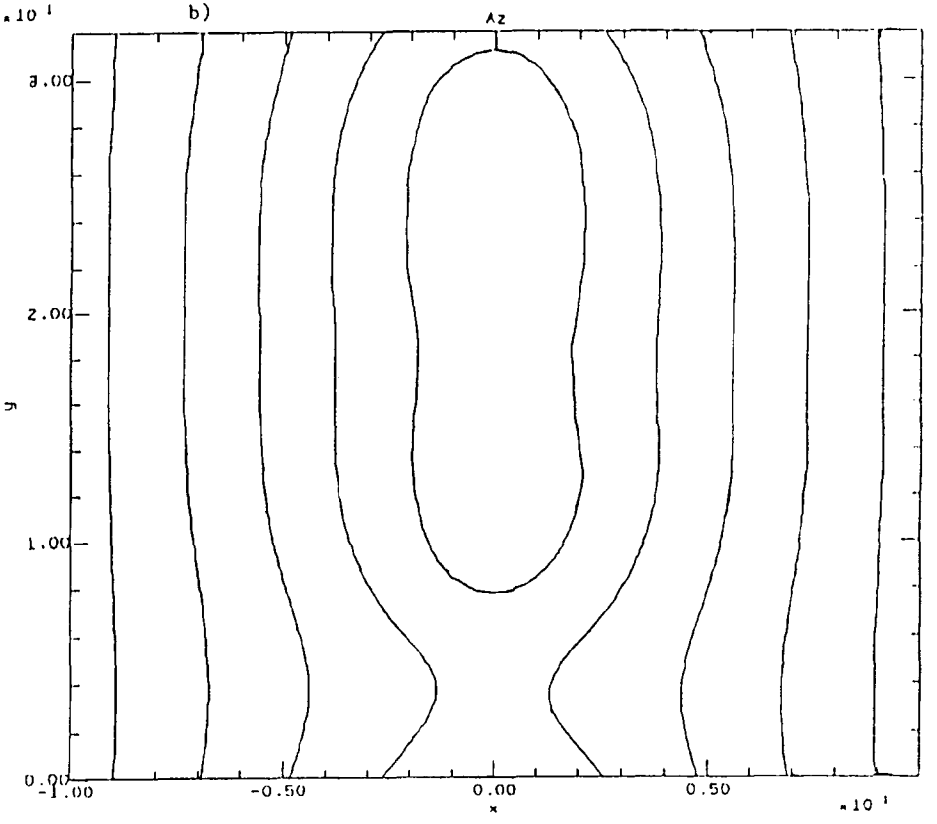
b)
Az
x
y